Ex-Situ and In-Situ Ellipsometric Studies of the Thermal Oxide on InP

X. Liu, J. W. Andrews, and E. A. Irene

Department of Chemistry,

University of North Carolina,

Chapel Hill, NC 27599-3290

Abstract

The thermally grown InP oxide as etched by an aqueous dilute HF solution has been studied by ellipsometric techniques. The ex-situ measurement reveals a two-layer structure for the oxide grown at 440^{0}C. The refractive indices for both oxide layers have been determined using a two-layer optical model. The etching process has also been monitored ellipsometrically in the real etching environment, in-situ. A fused silica cell, which enables the windows to be aligned properly, has been specifically designed for the in-situ solution measurement. A liquid layer at the solution-oxide interface has been identified, and the layer is shown to contain P and In species resulting from the etching reactions. A theory based on the Lorentz-Lorenz relation results in a reasonable qualitative description of the liquid layer. During the etching of the oxide the liquid layer shrinks at a linear rate, and after removal of the outer oxide layer the liquid layer forms a dense electric double layer.

Introduction

The surface oxide layer on semiconductor surfaces continues to attract considerable research effort. The recent applications in opto-electronics and microwave devices have drawn increasing attention towards InP. The oxide thermally grown on InP has been widely studied in an attempt to use it as an insulating material for the InP surface(1-7), as has been successfully accomplished for SiO_2 films on silicon. The chemical composition of the oxide has been found(5,7) to be both complicated and process dependent. Although some questions still remain, it is generally accepted that the oxide grown at low temperature($T < 600^0C$) is composed of two layers of differing chemical composition: an In-rich outer layer of a mixture of In_2O_3 and $InPO_4$ and an inner layer of predominantly $InPO_4$(8,9). Recently, spectroscopic ellipsometry has been applied (9,10) to examine the dielectric response of the InP thermal oxide, and the dielectric function in the energy range 2-5 eV for the oxide thermally grown at several temperatures has been reported.

Traditionally, the electric double layer formed at the solid aqueous solution interface has been studied using capacitance voltage measurements, potentiometric titrations, and microelectrophoresis methods(11). There are several investigations of the specific ion adsorption and the electric double layer using ellipsometric techniques(12,13). Several studies have focused on crystalline and amorphous SiO_2 immersed in an aqueous solution (14,15). Recently, Gould and Irene(16) have used in-situ ellipsometry to study the SiO_2 surface behavior dynamically by

monitoring changes in thicknesses and refractive indices of the oxide caused by a reactive solution, i.e. dilute aqueous HF, buffered HF, and aqueous NH_4OH/NH_4F, and Law(17) has reported observations of orientational ordering of water and organic solvents on pyrex surfaces by in-situ ellipsometry.

In this paper, we report an ex-situ ellipsometric study of the etch of an InP oxide thermally grown at 440^0C by a dilute aqueous HF solution. We show clear evidence for a two-layer structure for the oxide, and values for refractive indices for the outer and inner layer of the oxide at the wavelength of 632.8nm have been determined using a two-film optical model. We also describe an in-situ observation of the same etching system. A liquid layer, which has a different optical response than the bulk solution, has been found to be present at the oxide-solution interface during the oxide etching, and a microscopic model based on the Lorentz-Lorenz relation has been used to describe the liquid layer. In addition, we report the observation of an electric double layer at the solution-oxide interface which forms when the outer oxide layer is removed.

Experimental Procedures

N-type undoped (1 0 0) InP ($n<1.0x10^{16}cm^{-3}$) wafers were cut into 1x1 cm^2 samples. The samples were ultrasonically degreased in boiling trichloroethylene for 10 minutes, followed by a sequence of acetone, deionized water(d. i. water) rinse. After being dipped in a concentrated aqueous HF solution for 15 seconds, rinsed in d. i.

water, and dried in N_2 gas, the samples were loaded onto a fused silica boat. Then, the boat was placed in the end cap of the oxidation furnace for further drying, pushed into the hot zone for a 15 minute pre-oxidation annealing at 440^0C in a N_2 atmosphere, oxidized in 1 atm O_2 at 440^0C for 4 hours, and annealed in N_2 at the same temperature for 15 minutes.

A commercially available manual ellipsometer automated in our laboratory and shown in Fig. 1 consists of a HeNe laser, the light source, a quartz Rochon polarizer, a three-dimensionally adjustable sample stage, an autocollimating and alignment telescope(ACAT), a rotating analyzer, and a signal detection system. The ACAT is used for aligning the ellipsometer itself and samples to be measured. A Glan Tayor polarizing prism that is mounted on a hollow motor-driven shaft serves as the rotating analyzer. As the shaft rotates, an optical encoder generates pulses which trigger the analog to digital conversions. The periodic light signal through the analyzer is detected by a photomultiplier tube(PMT). The output PMT current, in turn, is converted to voltage, amplified to 0-10 volt range, and converted to a digital signal triggered by the encoder pulses. A dedicated personal computer controls the measurements.

A fused silica cell, as shown in Fig. 2, has been designed for the in-situ etching experiments. Two optically flat fused silica plates, serving as the entrance and exit windows, are connected to the main part of the cell through ball-socket joints, which enable the windows to be adjusted and then securely set in place. The

windows have to be orthogonal to the incident light beam for the solution measurements, otherwise the media with different indices of refraction on each side of the windows will alter the direction of the light beam, hence the angle of incidence, when the light beam passes through the windows. The solution inlet and outlet permit the changing of a solution without exposing the sample to air.

With a conventional analyzer in the position of the rotating analyzer, the ellipsometer and its optical components were aligned and calibrated as previously described(18). Then, the conventional analyzer was removed from the bench, and the rotating analyzer installed. The bench was set in a straight through(180^0) position and a series of measurements were carried out, and the offset correction for the rotating analyzer was determined from these measurements. Then, the incident angle was set to 70.00^0 for all the ellipsometry measurements.

The etchant used in both ex-situ and in-situ measurements was 1:500 HF(49%):H_2O solution. For the ex-situ measurements, the samples were dipped in the etchant for a certain time, rinsed in d. i. water, and blown dry by N_2 gas. Prior to an ellipsometric measurement, the sample was placed into a slot on the sample stage so that the same surface spot could be probed for the successive measurements, and the sample alignment was checked and adjusted if necessary. This process was repeated, with the etching times and ellipsometric parameters recorded.

The in-situ measurement first requires the alignment of the

solution cell. An sample was affixed with wax to a fused silica flat inside the cell, which was mounted on the adjustable stage. With both windows absent, the sample was aligned(19). Then, with the windows in place, the cell was filled with d. i. water, and the entrance window was aligned by adjusting the reflected beam from the window to coincide with the incident beam, and then the exit window was aligned independently. The first measurements after alignment were carried out in d. i. water to insure correct alignment, and then the dilute HF solution was rapidly introduced into the cell through the inlet while the water drained through the outlet. During the entire experiment, fresh HF solution was circulated into the cell at a rate of 7-9 ml/min. At the end of the experiment, the cell was drained, thoroughly washed with d. i. water, dried by N_2 gas, and several ellipsometric measurements were carried out in the air ambient.

Results and Discussion

A four phase model consisting of ideal optically isotropic and homogeneous phases: semi-infinite ambient - film 1 - film 2 - substrate, has been used in the ellipsometric data analysis for both ex-situ and in-situ experiments(20). For this optical system, there are three interfaces for reflection and two homogeneous and isotropic transmission layers involved. The reflection and transmission properties for each interface and each layer can be expressed individually by a characteristic 2x2 Jones matrix, and the overall properties of the multilayer structure can be obtained

from the product of these matrices(20). The relationship between the ellipsometric parameters Ψ and Δ, where Ψ is the change in the amplitude ratio, and Δ the change in the phase difference between the p and s components of a monochromatic polarized plane wave upon reflection from a surface, and the optical properties of the system is given by:

$$\tan \Psi \exp(j\Delta) = \rho(N_0, N_1, L_1, N_2, L_2, N_s, \phi, \lambda) \qquad (1)$$

where N_0, N_1, N_2, and N_s are the complex indices of the ambient, film 1, film 2, and the substrate, respectively. L_1 and L_2 are the thicknesses for the films. ϕ is the angle between the incident beam and the normal to the sample surface, and λ is the radiation wavelength. With the N_0, ϕ and λ as experimentally controlled variables, and with N_s fixed, with either N_1 and L_1 or N_2 and L_2 known, the other pair can be determined from the measured Ψ and Δ.

Later in the "In-Situ Ellipsometry Studies" part, we model a liquid layer as a medium with various ions and/or molecules near the oxide surface. For this purpose we assume a Lorentz-Lorenz relation which treats a film as composed of polarizable points. The measured refractive index can be related to the microscopic properties of molecules and ions which constitute the optical system by the Lorentz Lorenz equation(21). For a single component system, the equation can be expressed as:

$$\frac{4 \pi \alpha' N_A \eta}{3 M_w} = \frac{N^2 - 1}{N^2 + 2} \qquad (2)$$

where α' is the polarizability for a molecule or an ion, η is the density, and M_m and N_A are molecular weight and Avogadro's constant, respectively. With the assumption that the microscopic properties are additive, and for an isotropic and homogeneous phase consisting of m non-interacting components, the overall optical properties can be obtained in terms of the optical properties of the individual components(22):

$$\frac{N^2 - 1}{N^2 + 2} = \frac{4\pi}{3} \sum_{i=1}^{m} \gamma_i \alpha_i \qquad (3)$$

where γ_i and α_i are the volume fraction and polarizability for the i^{th} component, respectively, and N is the refractive index.

Ex-Situ Ellipsometry Studies

If the InP thermal oxide is treated as one homogeneous film, i.e. $L_1 = 0$, the film thickness(L_2) and refractive index(N_2) can be determined from the measured Ψ and Δ values of the ex-situ experiment. The calculated results versus the etching time have been plotted in Fig. 3 using the previously obtained value 3.521 + i0.300 for the complex refractive index of InP substrate(23). It is clear that the etch rate dramatically changes at around 90 seconds with the averaged etch rates before and after that point of approximately 17 and 0.5nm/min, respectively. The more than 30 times change in the etching rate indicates a significant difference in the chemical composition, i.e. a two-layer structure for the

oxide. The two-layer oxide structure is consistent with reported XPS analyses(8,9,24). Although the exact chemical composition of the InP thermal oxide is still unknown, it is generally accepted that the oxide is composed of an outer layer of a mixture of In_2O_3 and $InPO_4$ and an inner layer of predominantly $InPO_4$. It is apparent that the composition difference causes different etch rates for the InP thermal oxide by the dilute aqueous HF solution.

Due to the two-layer structure, the one-film model used for the calculations in Fig. 3 is valid only beyond 90 seconds. From Fig. 3, the thickness of the inner layer(L_2), of 12.2nm can be directly obtained as the thickness at the turning point, while the refractive index for this layer has been determined to be 2.09 by averaging the index values beyond that point and assuming a non-absorbing oxide for this wavelength, i.e. zero imaginary part for the index(9). Knowing L_2 and N_2, the thickness(L_1) and refractive index(N_1) for the outer layer have been determined to be 15.7nm and 1.94, respectively, according to equation (1). The final picture for the thermal oxide is given in the insert of Fig.3. As mentioned above, the one film model is only valid for the etch time greater than 90 seconds. For the initial region, calculations based on the two-film model have been carried out. Since results for the thicknesses of these points are only slightly different from the values shown in the Fig. 3 due to small difference in index, we will not address the thickness correction. Bergignat et. al. have measured the dielectric functions for InP thermal oxide grown in the 250 - 550^{0}C temperature range using spectroscopic

ellipsometry(9). An one film model was used in their data analysis for the thermal oxides grown at all temperatures except 550^{0}C, for which they used a two-film model. For the oxide grown at 450^{0}C, at the wavelength of 632.8nm, the refractive index was reported to be 1.86, which is lower than our values for either the inner or outer layer of the oxide grown at 440^{0}C. The difference may arise from the 10^{0}C difference in oxidation temperatures and/or a different value used in the data analysis for the complex refractive index of InP substrates. However, the index value used in their work can not be explicitly obtained.

In-Situ Ellipsometry Studies

The experimental Ψ and Δ values for the in-situ ellipsometric measurement of the thermally grown InP oxide etched by the dilute HF solution are shown in Fig. 4 along with calculated values. The calculated Ψ and Δ values assume constant refractive indices for films and substrate, and first a decreasing film thickness of the outer layer and then the inner layer and with both layers having a 14nm starting thickness. Since the etchant contains only 0.1 percent HF, the refractive index (1.3325) of pure H_2O at the wavelength of 632.8nm has been used for the dilute HF solution(25). The experimental starting point was at $\Psi = 15.04^0$ and $\Delta = 68.32^0$, and represented the sample under d. i. water prior to the HF etching, with a 14.4nm inner layer and 12nm outer layer. Another oxide sample grown similarly has been examined using the same etching procedure with a 2 minute time interval between successive

measurements and has yielded nearly identical results. As evident in the Figure, after the start point the measured data neither follow the calculated curve, nor approach the point for a bare InP substrate. It is apparent that a different mechanism other than simply film etching is involved. However, the above reported ex-situ results show the expected behavior for two-layer film etching. The oxide film roughening was expected to some degree during the prolonged etching. The effects of a rough film were estimated assuming a rough film with varying void percentage. It was found that the extremely rough film could not account for 10 percent of the digression of the measured Δ from the expected Δ. Thus, during the etching the sequence of events must include the formation of layers that cause large changes in polarized light in addition to the etching of the two-layer oxide film. In a separate study, a similar behavior was observed during HF etching of thermally grown SiO_2 on Si, but only after the oxide was etched away.

Considering the results above, a simple model for this new phenomenon would be a liquid layer sandwiched by the residual oxide and the bulk etchant. It is sensible to propose that there is a concentration gradient of etch products in the liquid layer extending from the etching oxide layer. With these assumptions, the dielectric response of this liquid layer is then calculated based on the Lorentz-Lorenz relation(22) which is appropriate for individual polarizable species. We shall proceed with the details of this calculation.

It should be understood that single wavelength ellipsometry

has restrictions in the modeling of an optical system(26). First, the dielectric response of the system may not be maximized at the wavelength 632.8 nm, hence the sensitivity may not be optimum. Secondly, by fitting a single measured point rather than a set of points, as would be the case for spectroscopic ellipsometry, the measurement errors can propagate through the modeling to the final result. As a consequence, the modeling can only be considered to have qualitative significance. However, knowledge gained about the sample before and after the in-situ etching has been used in the modeling, and we show that much of the ambiguity associated wit single wavelength ellipsometry can be eliminated.

From the ex-situ etching experiment above, we know that the etching of the outer layer of the oxide proceeded relatively fast. For the particular sample used in the in-situ measurement, the thickness of the outer oxide layer was about 12 nm. This thickness should be totally removed within a minute, leaving only the inner oxide after 5 minutes in the etching environment. The refractive index of 2.09 for the inner oxide, as determined in the above ex-situ measurement, has been used for the residual inner oxide. In addition, from measurements in air after the in-situ experiment, the thickness for the final residual oxide has been determined to be 7.1 nm. Using the two film model and starting from the last measured point of the in-situ data, with 2.09 and 7.1 nm as the refractive index and the thickness of the residual oxide on InP in the dilute HF solution, a 0.8 nm unknown top layer with an index of 3.07 is calculated to be between the bulk solution and the inner

oxide. We believe that this layer is a liquid layer because it disappears upon removal of the sample from the solution cell and subsequent d.i. rinse and blow dry. From this last point towards the beginning of the etching experiment, we assumed that the inner oxide is thicker. However, any significant increase in the thickness(L_2) beyond 7.1nm did not result in an acceptable model until the etching time was less than 15 minutes. Therefore, the thickness of the inner oxide has been fixed at L_2 = 7.1nm in the modeling for all the data points except for the initial two where L_2 has been determined to be 8.1 and 7.4nm, respectively, for the first and second points as the fitting parameters for the two film model. The modeling results for the liquid layer, L_1 and N_1, are summarized in Fig. 5. The initial 5 minute etch resulted in a 121 nm liquid layer with an index of 1.34, and the thickness of the liquid layer decreased quickly to about 1 nm at around 30 minutes while the index for the layer did not change significantly. Then, the thickness fluctuated slightly around 1 nm, and the index rose sharply for the next 10 minutes leveling off to a value greater than 3.0 after 120 minute etch. Figure 6 shows a diagram of this etching system, the liquid layer L_1 and oxide layer L_2.

In order to understand the nature of the liquid layer, the chemical reactions involved in the etching process should be considered. Since the HF solution can etch fused silica as well, the effects of the reaction of the HF solution with the cell needs to be evaluated. It has been reported that the etching rate of the fused silica by 1:500 HF(49%):H_2O was about 0.3 nm/min(16). For

the particular cell(150cm^3 in capacity) used in our experiments, the total number of SiO_2 molecules etched away from the cell was calculated to be 1.3 X 10^{15} per minute. Assuming that the etch products were SiF_6^{2-} ions, only 7.8 x 10^{15} F^- ions were consumed in one minute. For up to 1000 minutes, which are much longer than any of our in-situ measurements, 7.8 x 10^{18} F^- ions were consumed and 1.3 x 10^{18} SiF_6^{2-} ions were formed. Compared to the total amount of F^- ions in the cell, 5.1 x 10^{21}, the number of F^- ions consumed was negligibly small. The SiF_6^{2-} ions formed accounted for only 0.3 ppm. Hence, we conclude that neither the concentration nor the physical properties, i.e. refractive index, of the etching solution should be significantly affected by this process.

The behavior of the liquid layer as shown in Fig. 5, for the in-situ measurement before and after 30 minutes is distinctly different. Thus, we separately examine the two regimes. To start we consider that for the InP oxide etched by the aqueous HF three steps were involved: 1) F^- ions diffuse to the oxide surface, 2) F^- ions react with the outer layer of the oxide, and 3) the dissociated species diffuse away from the interface. Initially, the surface reaction proceeds at a relatively high rate as previously discussed, with the formation of significant amounts of ions and particles at the oxide surface and diffusing into the bulk solution. As a result, a concentration gradient is formed near the solution solid interface, which in turn causes the optical response in the in-situ ellipsometric measurement. Some possible reactions taking place at the oxide surface are:

$$In_2O_3 + 6H^+ = 2In^{3+} + 3H_2O$$

$$InPO_4 + 2H^+ = In^{3+} + H_2PO_4^-$$

$$P_2O_5 + 3H_2O = 2H_2PO_4^- + H^+$$

$$In^{3+} + 6F^- = InF_6^{3-}$$

A mixture of the ions such as H^+, F^-, In^{3+}, $H_2PO_4^-$, InF_6^{3-}, and solid particles such as $InPO_4$ and P_2O_5 in the vicinity of the oxide, can be imagined to constitute a concentration gradient in L_1 extending outward from oxide surface depicted in Fig. 6. If all the P and In species in the etch products are counted in the form of H_3PO_4 and InF_3, there would be approximately 1.42 and 4.02 x 10^{16} molecules, respectively, formed after the initial 5 minute etch. Assuming that these species are uniformly distributed within a distance from the solid surface, and beyond the distance, the concentration of the diffused species becomes negligible, an abrupt boundary can be defined as a plane parallel to the solid surface with a vertical distance as the measured thickness for the liquid layer and an area of the sample size, i.e. 1 cm^2. Using the Lorentz-Lorenz relation, the volume fractions for H_3PO_4 and InF_3 have been calculated, where 5.3 x 10^{-24} cm^3 has been used for the polarizability of H_3PO_4(27). We found no reference for the polarizability value of InF_3, so it was treated as a parameter. For these specific calculations, 4.4 x 10^{-24} cm^3 has been used, and it was found that the numerical value did not qualitatively affect the calculations. Relative to the total amount of the P and In species formed, the percentage of the moleculars remaining in the boundary has also been calculated. Similar treatments have been carried out for several other points

and summarized in Table 1. The first row of the table lists the etching time, and the second and the third are the thicknesses and refractive indices, respectively, for L_1 from Fig. 5. The total amounts of P and In species produced by the etch in the forms of H_3PO_4 and InF_3 are listed in the fourth and fifth, respectively. These values were obtained by counting the numbers of the In_2O_3 and $InPO_4$ molecules in the oxide before they were etched away. The bottom row is the percentage of total etch products remaining in the liquid layer. As shown in the table, the refractive indices and volume fractions for both species, did not change much before 25 minutes of etching time, while the thickness and the percentage of etch products remaining in the layer decreased steadily. The percentage of the remaining etch species and liquid layer thickness from Table 1 were plotted versus the etching time in Fig. 7a and 7b, respectively. Fig. 7a shows a linear decrease of the total etch products remaining in the liquid layer, while Fig. 7b shows that the liquid layer decreases linearly from 10 to 20 minutes, then falls at an even faster rate. The Maxwell-Garnett effective medium approximation treatment, in which the etch solution was considered as a host medium(H_2O) containing dissociated particles (H_3PO_4 and InF_3), has also been carried out to examine the liquid layer and similar to the Lorentz-Lorenz results we found a linear decrease in the percentage of both total P and In remaining in the liquid layer. However, the value for the first point and the slope of the linear decrease were much lower than that from Lorentz-Lorenz treatment. With this modeling, the physical picture of this

particular etching phenomenon becomes clear. Initially, the surface reaction of F^- with the oxide proceeds relatively fast, and the etch products diffusing away from the oxide surface form a thick liquid layer in a short time. After the removal of the outer oxide layer, the reaction slows down and eventually stops, and so does the supply of the P and In species. Thus, the out diffusion of these species becomes dominant due to the circulation of the HF solution, which maintains a constant concentration in the bulk solution, and transports the out-diffused species out of the cell. The liquid layer starts to shrink slowly and then at a linear rate. After 20 minutes, as shown in Fig. 7b, the liquid layer thickness drops at a higher rate. The linear decrease of the thickness from 10 to 20 minutes can be described by:

$$L = 169 - 5t; \qquad (4)$$

where L is the thickness of the liquid layer in nanometers, and t is the etching time in minutes. Equation (4) also represents the rate at which the etch products diffuse out of the surface region.

So far, we have modeled the in-situ ellipsometric data for HF etching InP oxide and established a simple physical picture for the complex etching system. If we keep a constant refractive index for the liquid layer, 1.34 in this case, vary the thicknesses according to equation (4), and use the same inner oxide layer as described above and the two film model, the Ψ and Δ can be obtained, in Fig. 8, curve b. The calculated data for a two layer oxide in H_2O of Fig. 4 is shown again in Fig. 8 as curve a. Before the introduction of HF solution, the measured Ψ and Δ point was close to curve a, then

the measured data jumped onto curve b(see Fig. 4) and followed it very closely up to 30 minutes in the etching solution. Afterwards, the measured data departed from curve b. The deviation can be accounted for by considering the contraction of the liquid layer and will be discussed below.

Before we proceed to the next regime of the in-situ measurement, we need to examine and evaluate the assumptions and approximations made in the above discussion. Firstly, we have assumed that an abrupt boundary layer existed. Within the boundary layer, the ions and solid particles were uniformly distributed, while outside it, there were negligible amounts of ions and particles. Therefore, an isotropic and homogeneous optical layer could be assumed in the two film model. This is obviously only a rough approximation of a continuous concentration gradient. However, because of the low concentrations and the gradual change from the oxide surface to the bulk solution, the optical properties, i.e. refractive index, for both sides of the boundary were only slightly different, we believe that this is a reasonable approximation for this particular system. Secondly, the P and In species formed were accounted for as only H_3PO_4 and InF_3, with the estimated polarizability values for H_3PO_4 and InF_3 having been used in the calculation. In reality a large number of species may exist in solution and each individual species is expected to be different in optical respones. Nevertheless, the physics and the qualitative meanings of our simple treatment is a useful average way to treat the complex system. The third assumption was that we neglected the

surface roughness, surface electrical charge distribution, ions adsorbed by the oxide, as well as alignment of the H_2O molecules along their permanent dipole moments in the vicinity of the solid surface. All these factors could affect the observed results in one way or another, but apparently from the success of the simple model none of them predominated.

Beyond 30 minutes, a different mechanism was dominant. As the thickness of the liquid layer decreased quickly to about 1 nm, the refractive index markedly increased and then leveled off as shown in Fig. 5. The rapid contraction of the liquid layer suggests that certain ions and/or molecules have been driven towards the solid surface, and formed a dense liquid layer. The layer condensed slowly for about 95 minutes and eventually saturated. Curve c of Fig. 8 are calculated data for a 1 nm liquid layer on the residual oxide with a varying index for the liquid layer. The fit of this curve to the rest of the measured data supports our ellipsometric modeling for this regime, as seen by the experimental data in Fig. 4 with the model in Fig. 8.

The driving force for the condensation is likely electrical in nature, and possibly results from either the net electrical charges in the residual oxide due to the removal of the counter charges resident in the outer oxide, or the specific ion adsorption by the inner oxide, or both. Applying the previous results from the two film modeling to the electric double layer, the thickness and refractive index are found to be 1.0 nm and 3.1, respectively. As for comparision, the thickness and refractive index of the double

layer in the second measurement are determined to be 1.2nm and 2.8, respectively. Stedman(12) has reported an investigation of the electric double layer formed at a metal electrolyte interface using ellipsometric techniques, and a simple theoretical treatment was also discussed. The optical response of the components of the electric double layer was examined separately in that work. The inner layer consisted of compressed solvent dipoles that resulted in a larger refractive index than the bulk solvent. The ions adsorbed on the solid surface and the ions in the Gouy Chapman diffuse layer also contributed to the observed optical response. The type of ions and their distribution in the electric double layer determined the dielectric properties. In principle, the refractive index can be estimated using the Lorentz-Lorenz equation if the concentration of the adsorbed ions and ion distribution in the diffuse layer is known. As discussed above, the system of the HF etching InP oxide is complicated. A variety of ions were formed and contributed to the electric double layer. However, the detail knowledge about the structure of the electric double layer, which is essential for the estimation of the refractive index, could not be obtained by the ellipsometric technique alone. It would be valuable to combine electrochemical techniques for the study of the solution-solid interfacial phenomena.

Conclusions

The InP oxide surface reaction with a dilute HF solution has been studied by both ex-situ and in-situ ellipsometric techniques.

The two-layer structure for the thermally grown InP oxide has been clearly identified and characterized. The outer layer of the oxide which has a lower refractive index was etched much faster than the inner layer which has a higher index value.

A two-layer optical model has been used to analyze the in-situ etching ellipsometry data. A liquid layer consisting of the etch products of P and In species has been detected for the initial regime. Based on the Lorentz-Lorenz relation, a microscopic model has been established to describe the liquid layer. A linear process can account for the out diffusion of the etch species, which forms the liquid layer. The theory agrees qualitatively with our experimental results. An electric double layer was observed to form at the oxide-solution interface. The thickness and refractive index for the double layer has been estimated as 1.0 nm and 3.1, respectively. With the sensitivity of ellipsometry, in-situ solution ellipsometry is a promising technique for the study of the solid-solution interface phenomena.

Acknowledgement

This research was supported in part by the Office of Naval Research, ONR, and the Semiconductor Research Corporation, SRC.

Reference

1. J.F. Wager, D.L. Ellsworth, S.M. Goodnick, and C.W. Wilmsen, J. Vac. Sci. Technol., 19, 513 (1981).

2. C.W. Wilmsen, Thin Solid Films, 39, 105 (1976).

3. C.W. Wilmsen, K.M. Geib, R. Gann, J. Costello, G. Hryckowian, and R.J. Zeto, J. Vac. Sci. Technol., B3, 1103 (1985).

4. G. Hughes and R. Ludeke, J. Vac. Sci. Technol., B4, 1109 (1986).

5. G.P. Schwartz, W.A. Sunder, and J.E. Griffiths, Appl. Phys. Lett. 37, 925 (1980).

6. J.F. Wager and C.W. Wilmsen, J. Appl. Phys., 51, 812 (1980).

7. O.R. Monteiro and J. W. Evans, J. Electrochem. Soc., 135, 2366 (1988).

8. A. Nelson, K. Geib, And C.W. Wilmsen, J. Appl. Phys., 54, 4134 (1983).

9. E. Bergignat, G. Hollinger, and Y. Robach, Surf. Sci., 189/190, 353 (1987).

10. Y. Robach, A. Gagnaire, J. Joseph, E. Bergignat, and G. Hollinger, Thin Solid Film, 162, 81 (1988).

11. J.A. Davis, R.O. James, and J.O. Leckie, J. Colloid Interface Sci., 63, 480 (1978).

12. M. Stedman, In Optical Studies of Adsorbed Layers at Interfaces, University Press, Aberdeen, G.B., 1971, P64.

13. F. Meyer, and M.J. Sparnaay, ibid., P17.

14. R.J. Hunter, and H.J.L. Wright, J. Colloid Interface sci., 37, 564 (1971).

15. TH.F. Tadros, and J. Lyklema, J. Electroanal. Chem. 17, 267 (1968).

16. G. Gould and E.A. Irene, J. Electrochem. Soc., 135, 1535 (1988).

17. B.M. Law, J. Colloid Interface Sci., 134, 1 (1990).

18. F.L. McCrackin, E. Passaglia, R.R. Stromberg, H.L. Steinberg, J. Res. of N.B.S.A., 67A, 363 (1963).

19. D.E. Aspnes and A.A. Studna, Phys. Rev. B, 27, 985 (1983).

20. R.M.A. Azzam and N.M. Bashara, Ellipsometry and Polarized Light(North- Holland), 1977, P.339.

21. H.A. Lorentz, Theory of Electrons, 2nd ed.(Teubner, Leipzig), 1916, Chap. 4.

22. D.E. Aspnes, Am. J. Phys., 50, 704 (1982).

23. X. Liu, E.A. Irene, S. Hattangady, and G. Fountain, J. Electrochem. Soc., 137, 2319 (1990).

24. G. Hollinger, E. Bergignat, J. Joseph, and Y. Robach, J. Vac. Sci. Technol., A3, 2082 (1985).

25. P.W. Atkins, Phys. Chem., 3rd ed.(Freeman, New York), 1986, P581.

26. D.E. Aspnes and A.A. Studna, SPIE Vol. 276, 227 (1981)

27. J. Timmermans, the Physico-Chemical Constants of Binary Systems (Interscience, New York), Vol. 4, 1960, P526.

List of Figures

Figure 8: The in-situ measured data(open circles) and three simulated curves labelled a, b, and c. Curve a is calculated assuming a two layer oxide as in Figure 4, curve b assuming a constant index and a linearly changed thickness for the liquid layer, and curve c for a 1 nm liquid layer with variable index.

List of Tables

Table 1: A summary of the calculations of the volume fractions for P and In species in the liquid layer for the etching time 5 to 30 minutes. All the P species have been counted in the form of H_3PO_4, and In species in InF_3.

Figure 1

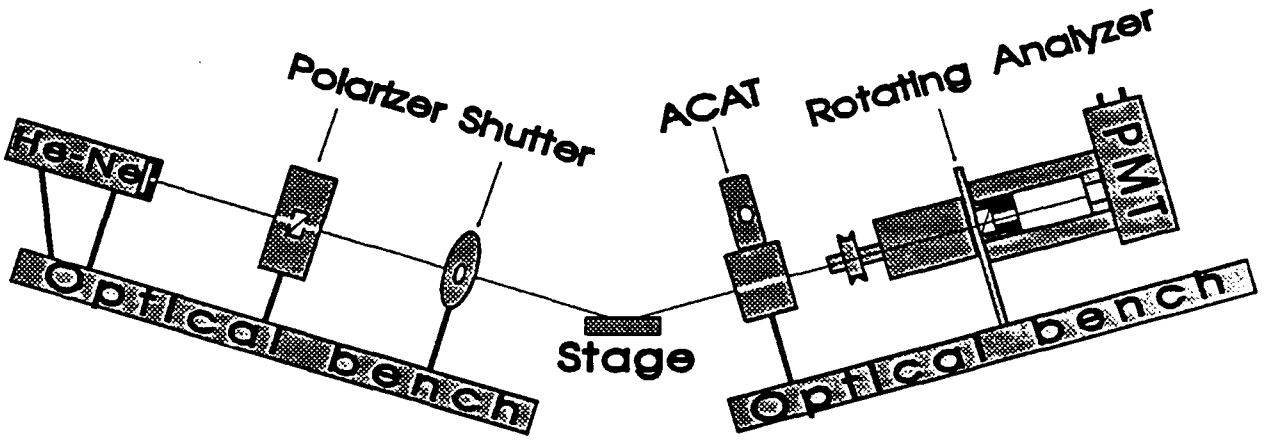
He-Ne
Polarizer
Shutter
ACAT
Rotating Analyzer
PMT
Optical bench
Stage
Optical bench

Figure 2

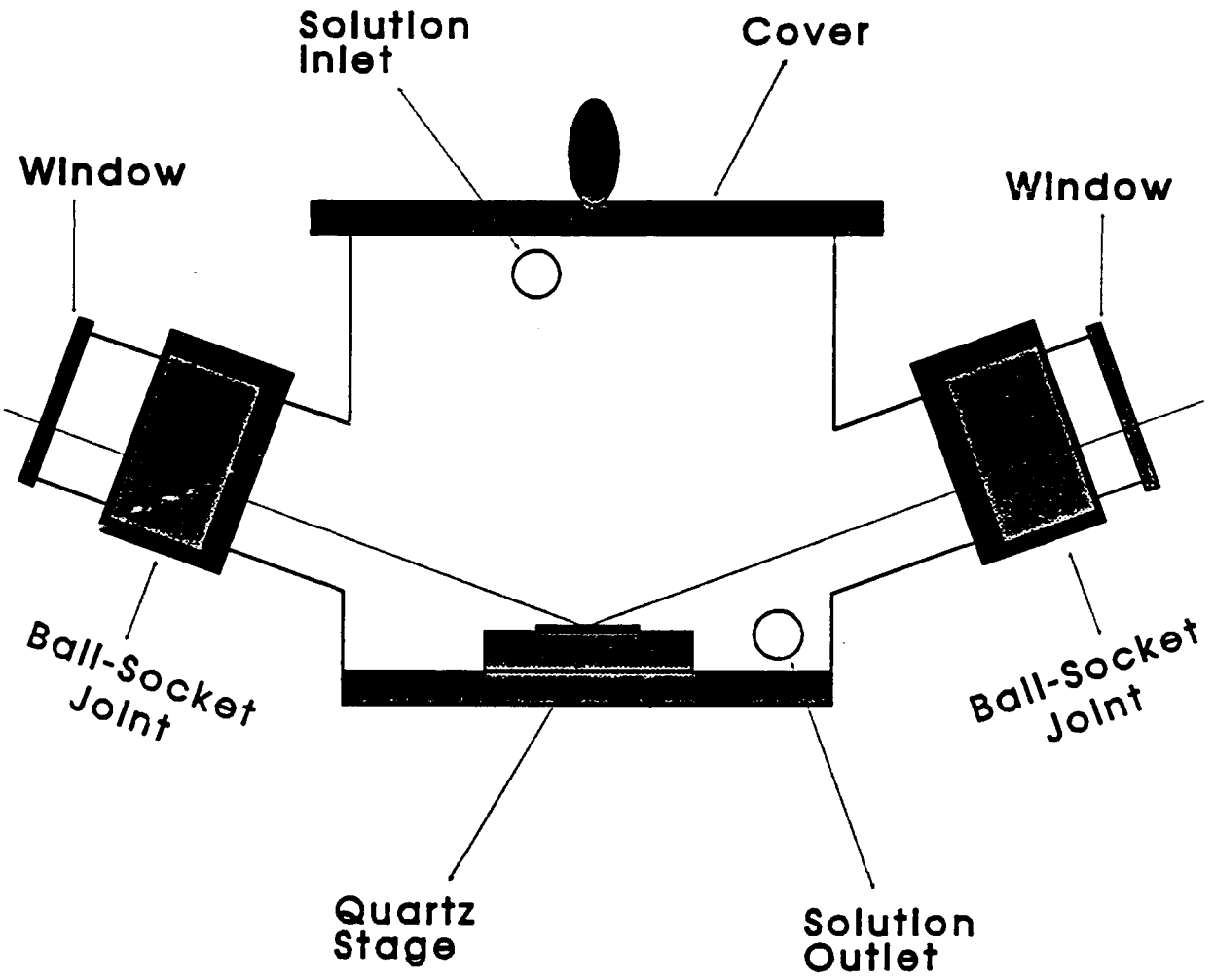
Solution
Inlet
Cover
Window
Window
Ball-Socket
Joint
Ball-Socket
Joint
Quartz
Stage
Solution
Outlet

Figure 3

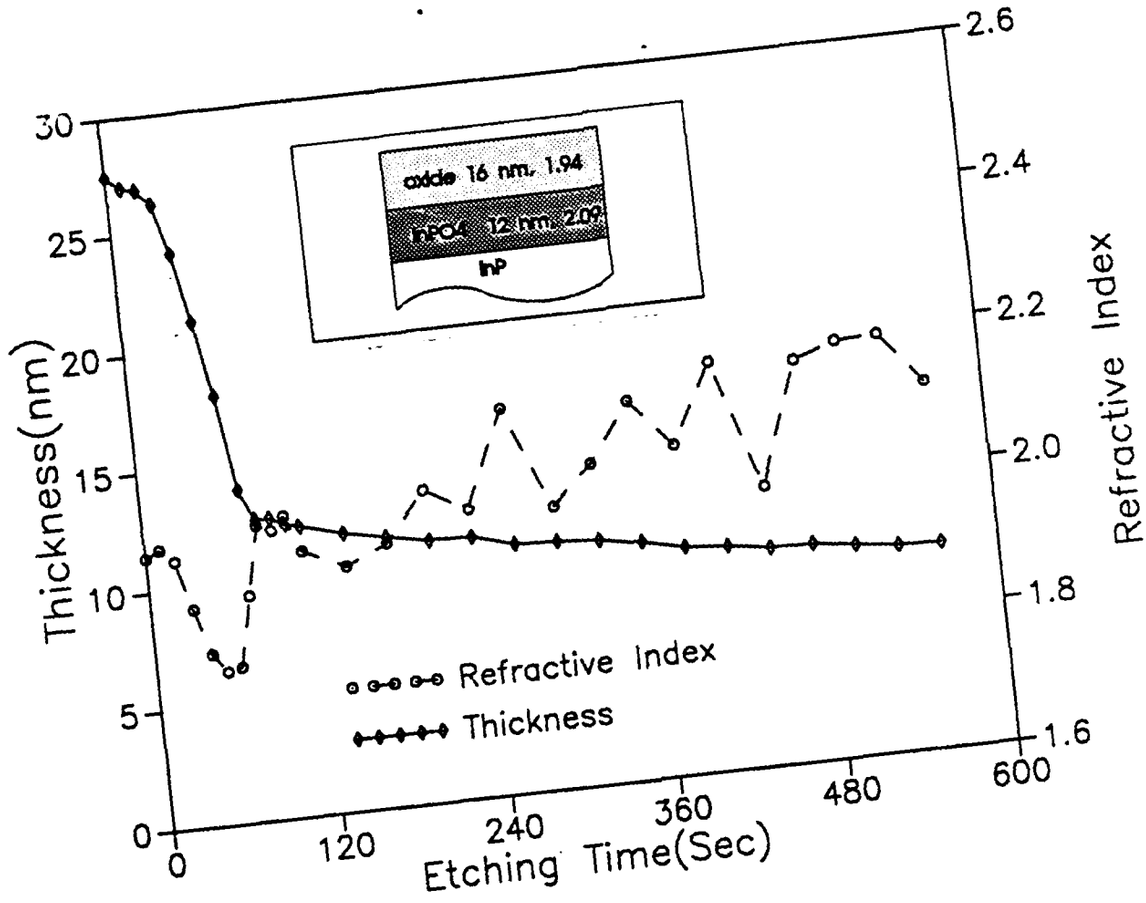
oxide 16 nm, 1.94
InPQ4 12 nm, 2.09
InP
Thickness(nm)
Refractive Index
Etching Time(Sec)
Refractive Index
Thickness
0
5
10
15
20
25
30
1.6
1.8
2.0
2.2
2.4
2.6
0
120
240
360
480
600

Figure 4

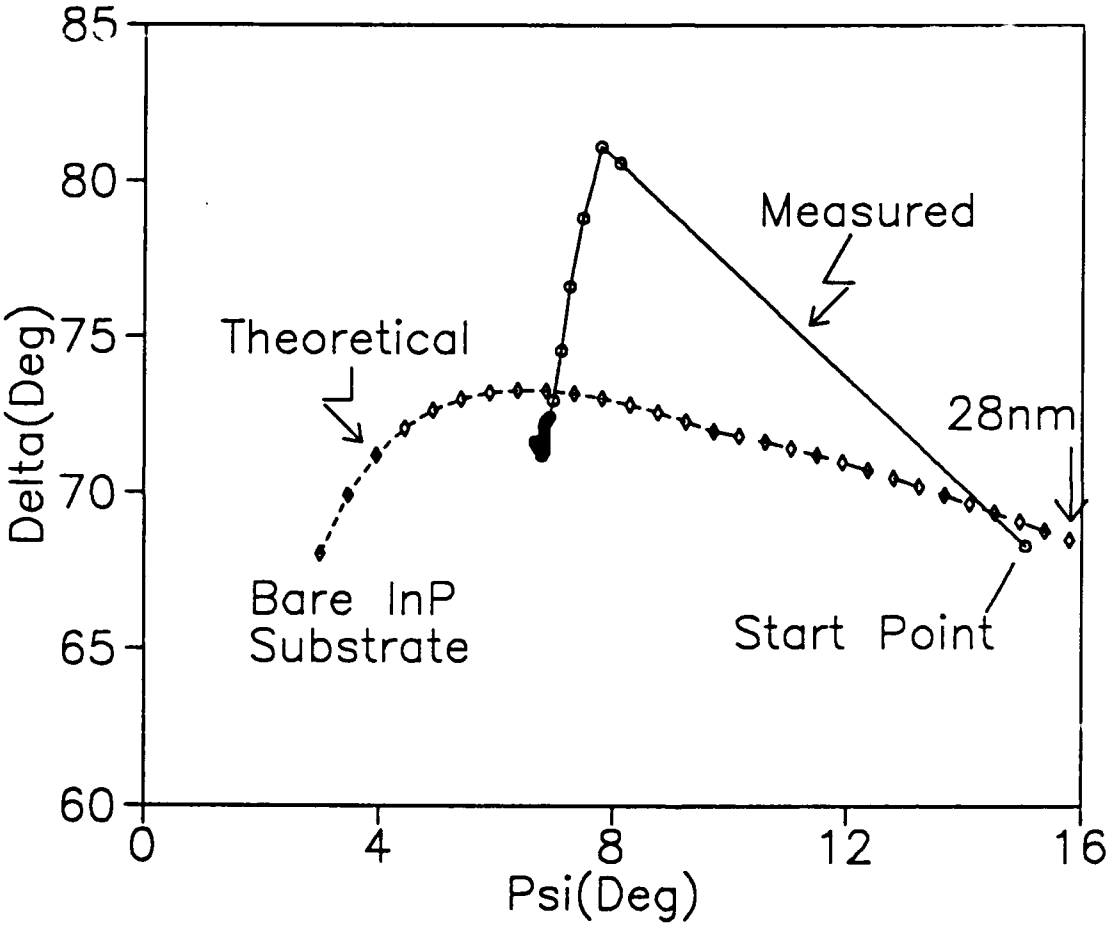
85
80
75
70
65
60
Delta(Deg)
0
4
8
12
16
Psi(Deg)
Measured
Theoretical
28nm
Bare InP
Substrate
Start Point

Figure 5

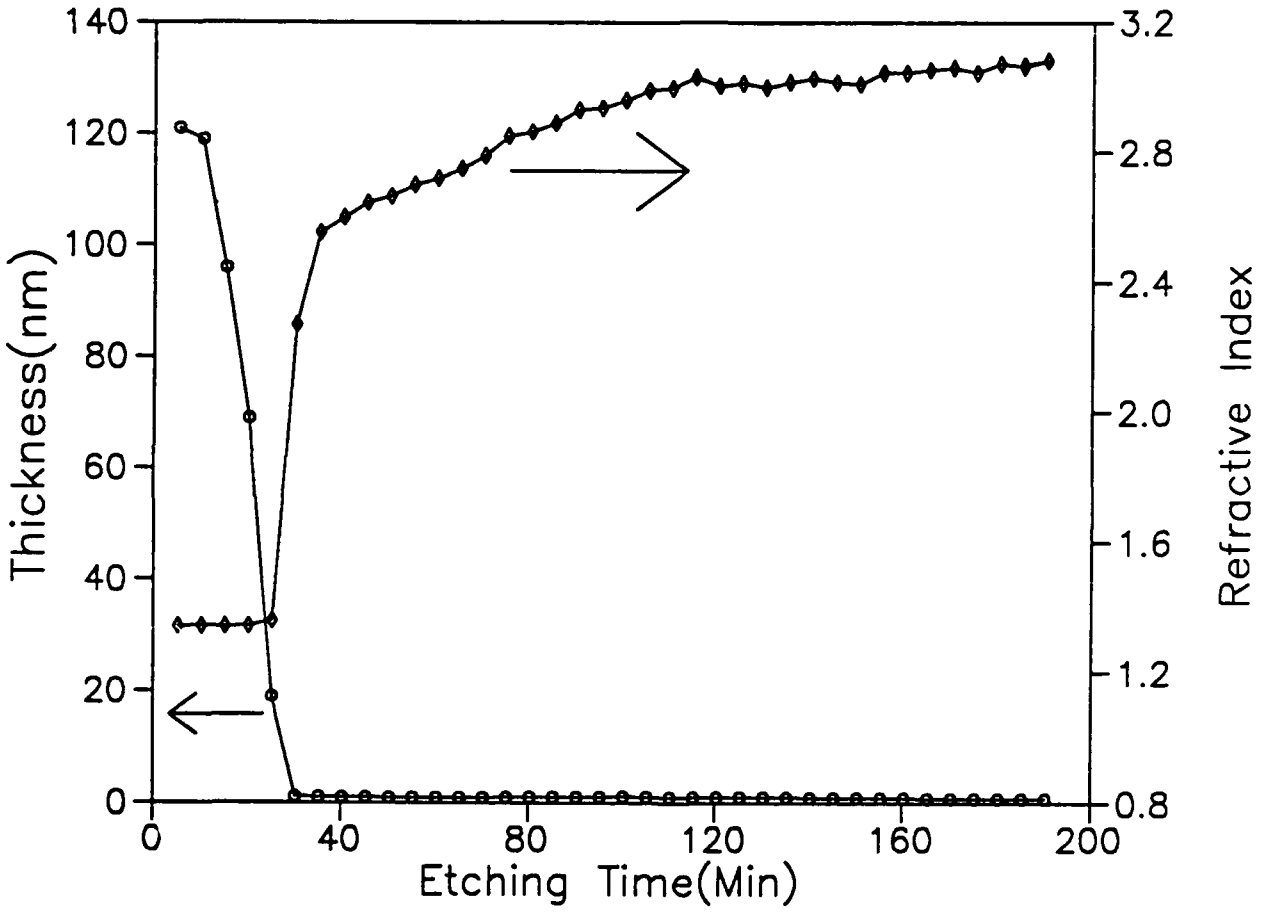
140
120
100
80
60
40
20
0
Thickness(nm)
3.2
2.8
2.4
2.0
1.6
1.2
0.8
Refractive Index
0
40
80
120
160
200
Etching Time(Min)

Figure 6

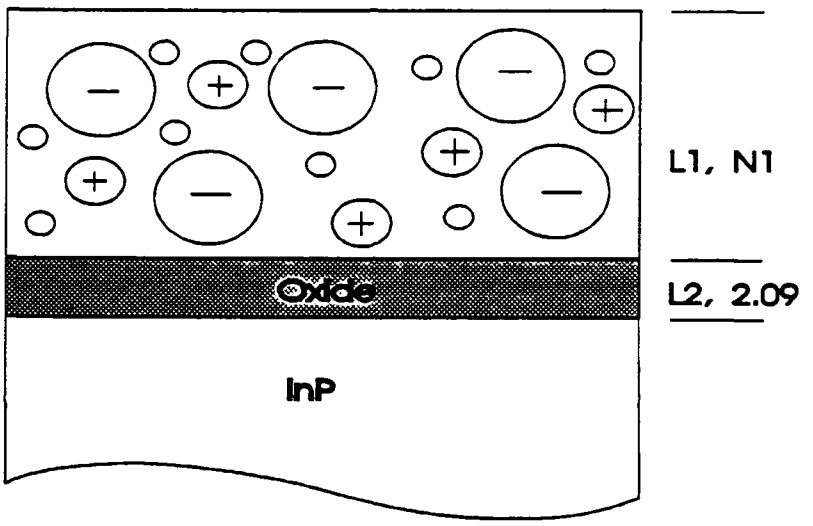

Figure 7

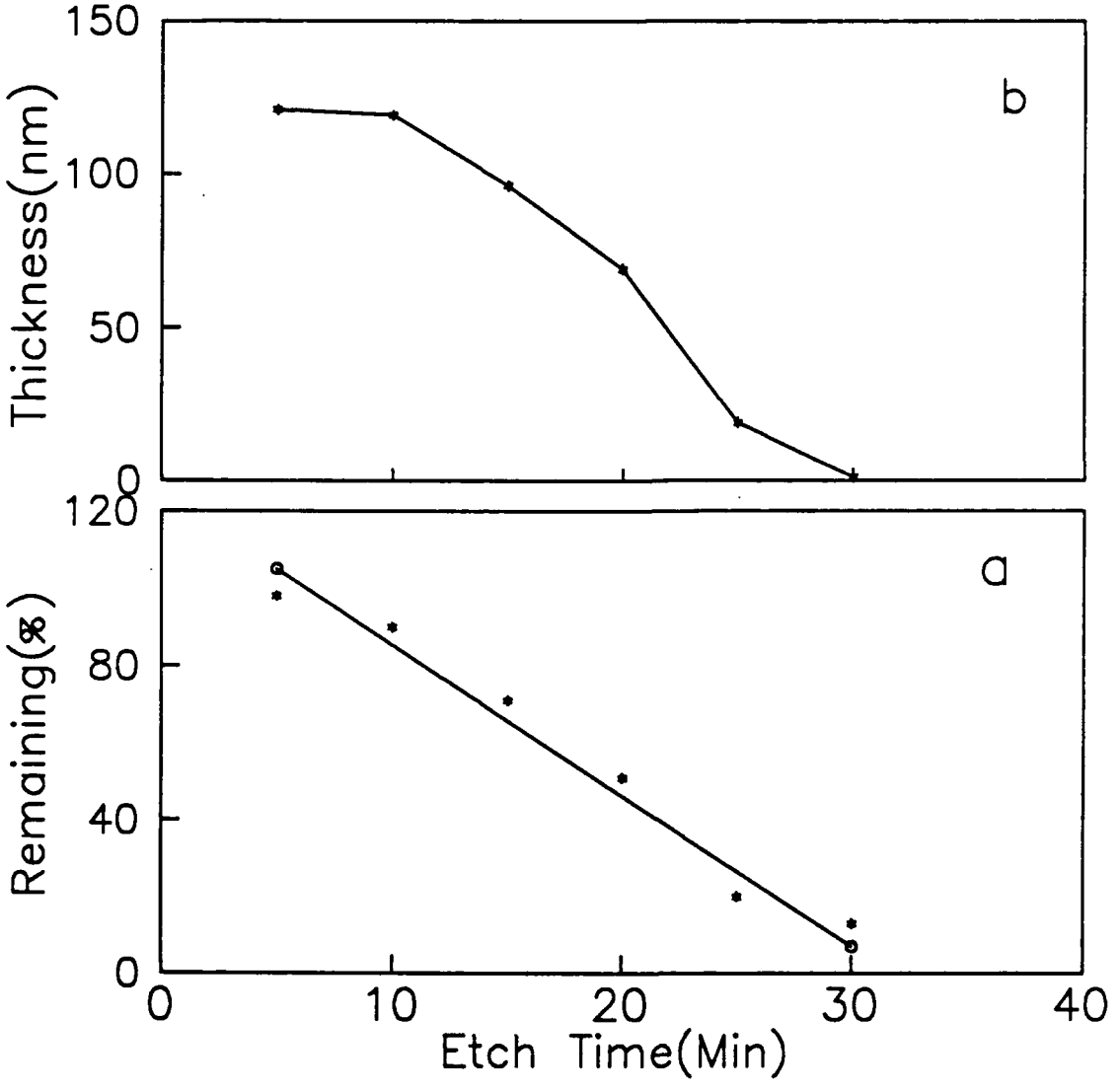
150
100
50
0
Thickness(nm)
b
120
80
40
0
Remaining(%)
a
0
10
20
30
40
Etch Time(Min)

Figure 8

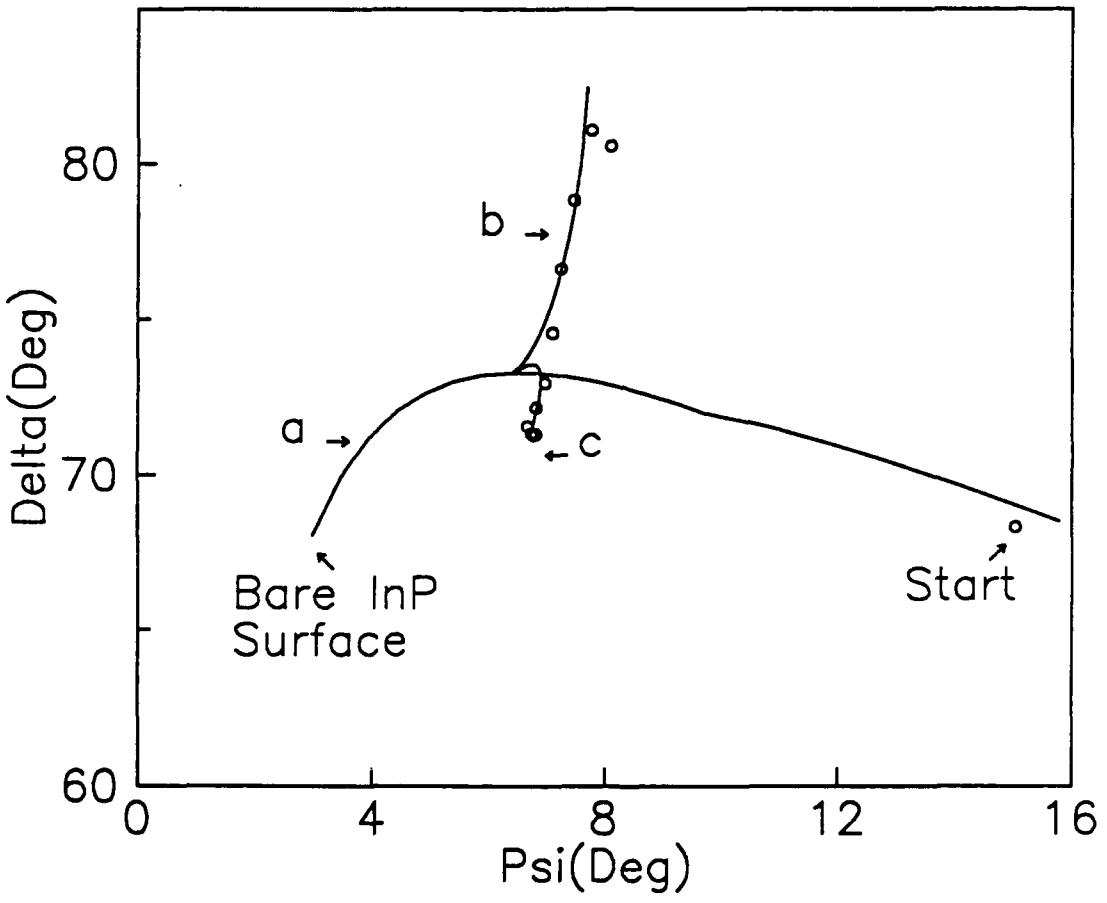

Table 1

Time (Min)	5	10	15	20	25	30
Exp. Thickness (nm), L_1	121	119	96	69	19	1.2
Exp. Index, N_1	1.34	1.34	1.34	1.34	1.36	2.27
H_3PO_4 ($x10^{16}$)	1.42	1.49	1.52	1.52	1.52	1.52
InF_3 ($x10^{16}$)	4.02	4.14	4.19	4.19	4.19	4.19
Remaining (%)	98	90	71	51	20	13